AIP | Applied Physics Letters

A robust polymer microcable structure for flexible devices

Eric Kim, Hongen Tu, Cheng Lv, Hanqing Jiang, Hongyu Yu, and Yong Xu

Citation: Applied Physics Letters **102**, 033506 (2013); doi: 10.1063/1.4788917
View online: http://dx.doi.org/10.1063/1.4788917
View Table of Contents: http://scitation.aip.org/content/aip/journal/apl/102/3?ver=pdfcov
Published by the AIP Publishing

A robust polymer microcable structure for flexible devices

Eric Kim,[1] Hongen Tu,[1] Cheng Lv,[2] Hanqing Jiang,[2] Hongyu Yu,[3] and Yong Xu[1,a)]
[1]*Electrical and Computer Engineering, Wayne State University, 5050 Anthony Wayne Dr, Detroit, Michigan 48202, USA*
[2]*Mechanical Engineering, School for Engineering of Matter, Transport and Energy, Arizona State University, Goldwater Ctr., Rm 302, 650 E. Tyler mall, Box 878406, Tempe, Arizona 85287, USA*
[3]*School of Electrical, Computer and Energy Engineering, Arizona State University, Goldwater Ctr., Rm 302, 650 E. Tyler mall, Box 878406, Tempe, Arizona 85287, USA*

(Received 14 September 2012; accepted 27 December 2012; published online 24 January 2013)

This letter reports a parylene cable structure that can significantly increase the robustness of flexible devices based on a silicon-island structure. In our previous work, it has been observed that the flexible cables connecting silicon islands could experience stress concentration at the edge of the silicon islands and fracture the metal traces. To address this issue, a micro cushion structure based on parylene micro-channels is proposed to minimize the stress concentration. This structure also improves the overall mechanical strength of the cables, and provides a simple method to encapsulate metal traces reliably. © *2013 American Institute of Physics*. [http://dx.doi.org/10.1063/1.4788917]

Over the last few decades, advances in flexible electronics and sensors have revealed a fantastic potential for various medical applications. A number of different flexible electronics/sensors technologies have been developed. The traditional way is to fabricate electronics and sensors directly on flexible substrate using low-temperature processes. Flexible printed circuit boards (PCBs), thin film transistors (TFTs) on flexible substrates, and a few thin film sensors have been fabricated using this method.[1–3] In addition to traditional microfabrication techniques, printing methods have also been widely used.[4–8] The main disadvantage of the above methods is the temperature limit, which rules out high temperature materials and processes, resulting in constrained functionality.

A few years ago, an innovative "transfer printing" method to make flexible electronics was demonstrated.[9–12] With this method, transistors and other devices are fabricated first on silicon-on-insulator (SOI) wafers and then transferred to flexible substrates by "printing" using elastomeric stamps. A number of exciting biomedical applications have been demonstrated with this technology.[13–15] Nevertheless, the transfer printing step may limit the yield and is not completely compatible with commercial complementary metal-oxide-semiconductor (CMOS) processes. Therefore, this method cannot fully take advantage of the mainstream CMOS technology.

We have demonstrated a different flexible skin technology based on silicon island structure.[16–18] The major advantage of this technology is its compatibility with micro-electro-mechanical system (MEMS) and CMOS since MEMS devices and CMOS circuits can be fabricated on the silicon wafer before the formation of the flexible skin. By taking advantage of CMOS foundries, complicated high-performance circuits can be integrated economically. As shown in Fig. 1, the basic structure of the flexible skin is an array of silicon islands sandwiched by two layers of polymer.

A large variety of devices, such as flexible shear stress sensor skins,[16] flexible sensor skins integrated with CMOS circuits,[17] intelligent textiles,[18] 3-dimensional (3D) neural probes,[19] and flexible microtube devices for neurotransmitter-based retinal prosthesis[20] have been demonstrated using this technology. It has been observed that the edge of the silicon island, where the flexible polymer cables interface with the rigid silicon, is a stress concentration area and may cause the fracture of the metal traces there. This issue becomes more severe when the polymer is parylene, which has fairly low melting temperature.

To address this issue, we proposed an innovative cushion structure to minimize the stress concentration at the silicon island edge. As shown in Fig. 2, there is a micro-channel between the metal trace and the rigid silicon edge, which functions as a cushion to minimize the stress concentration. This structure is realized by taking advantage of XeF_2 (xenon difluoride) gas phase isotropic silicon etching and parylene conformal coating.

To prove the concept, we designed our test devices to be pairs and 3×3 arrays of square silicon islands connected to each other by four serpentine-shaped parlyene microcables. Aluminum traces and contact pads formed a conductive network for electrical testing. For the pairs of islands, traces were patterned such that a square contact pad on one island connects to a neighboring pad on the same island via the route that travels through a serpentine microcable between two islands, across a wide trace on the opposing island, and through another serpentine microcable between two islands.

The process flow of the robust cable structure is shown in Fig. 3. The process is started with thermal oxidation on a

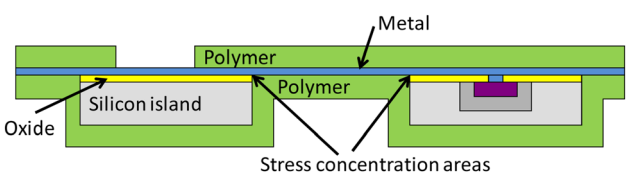

FIG. 1. Cross sectional schematic of flexible sensors/electronics based on silicon island structure.

a)Author to whom correspondence should be addressed. Electronic mail: yxu@eng.wayne.edu.

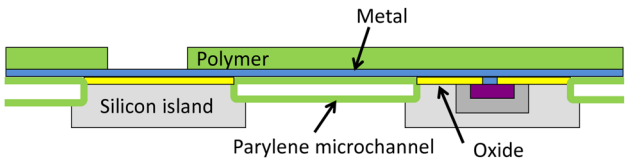

FIG. 2. Cross sectional schematic of the robust cable structure for silicon island based flexible devices.

300 μm thick 4 in. silicon wafer using PWS oxidation furnace. The resulting 0.5 μm oxide layer was then patterned using a photoresist mask (EVG-620 mask aligner) and a buffered oxide etch so that oxide is present everywhere on the intended silicon islands except buffer regions 80 μm from the boundaries of the islands. This non-oxide covered zone provides the region in which our channel structures can be formed. Then, a 220 nm thick aluminum layer was evaporated (Temescal Model BJD-1800 e-beam evaporator) and patterned. Next, a 5 μm parylene C layer was vapor-phase deposited using a SCS PDS 2010 parylene deposition system. Parylene is the generic name of poly-para-xylylene, which can be conformally deposited at room temperature. Note that we have previously used parylene C as a cantilever material[21–23] and the substrate for flexible sensors and electronics.[17,19] The parylene C layer is then patterned using oxygen plasma (DryTech RIE 184) to open small rectangular holes 10 μm apart and 8 μm wide in a row along the intended center of our parylene channel. These holes in the parylene C served as the mask for the XeF_2 etch to form the parylene channel mold trenches. The silicon substrate was then undercut via these holes by XeF_2, a gas phase isotropic silicon etchant, forming a trench underneath the metal trace. Due to the isotropic nature of the XeF_2 etching, the trench formed has a cross section close to a semi-circle. In the next step, the second parylene C layer was deposited. Note that parylene deposition is very conformal. Consequently, this parylene layer is deposited on the trench surface and seals the access holes in the first layer of parylene, leading to a sealed channel with a semi-circular cross section. The trench actually serves as a mold for the parylene channel. Then, the front side parylene was patterned by oxygen plasma to shape the outline of the device and open contact pads. Backside deep trench

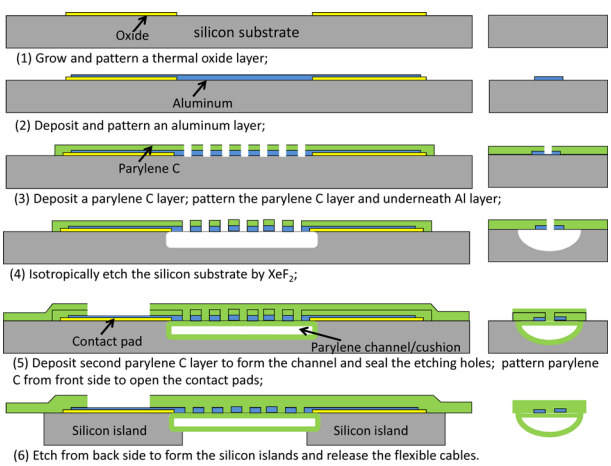

FIG. 3. Process flow of the robust cable structure for silicon island based flexible skins. The right column illustrates the cross sectional views along the transverse direction of the cable.

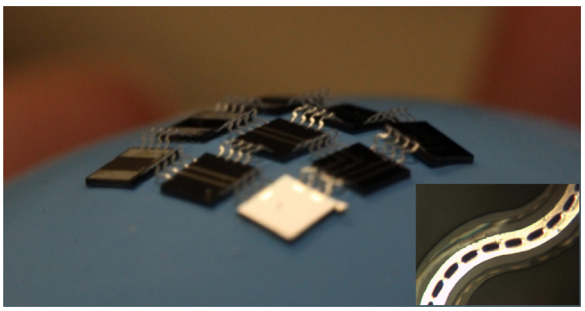

FIG. 4. A flexible device of 3 × 3 silicon island array compressed on the surface a balloon (inset: optical micrograph of a serpentine section in the middle of the cables).

etching was performed (Plasma-Therm 790 SLR series) to define individual silicon islands and releasing the parylene microcables.

Fabrication of these devices was of very high yield (around 90%). The addition of the parylene channel offers a more robust sealing of the metal traces in the microcables, and it offers reinforcement that protects them during post processing, handling, and setup. Compared to control devices without underlying parylene channels, test devices were qualitatively far more robust, being more stiff versus weak forces such as gravity and vibrations. Figure 4 shows a device of 3 × 3 array of silicon islands, which are connected by serpentine-shape cables, compressed in lateral direction on the spherical surface of a balloon. The buckled cables can be clearly observed. The silicon islands for the array have dimensions of 2.5 mm × 2.5 mm × 0.3 mm and the distance between islands is approximately 1.5 mm. Dimensions for the two-island devices are 2 mm × 2.5 mm × 0.3 mm with 2 mm gaps between them.

Figure 4 inset shows an optical micrograph of the serpentine cable. The aluminum in the center trace reflects the light and appears white. The etching holes for the XeF_2 undercut were formed along the center line of the metal trace. Parylene C is transparent. The channel approximately has a semi-circular cross section. On the topside, the sidewall of the semi-circular channel can be observed due to the different thicknesses. Figure 5 shows the anchoring section of the cable at the edge of the silicon island. It is worth noting

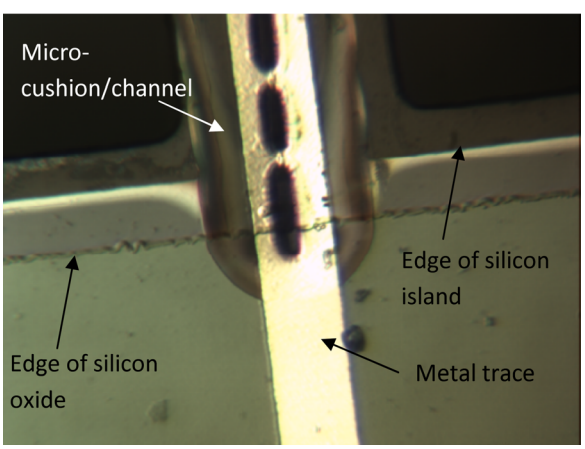

FIG. 5. Optical micrograph of the flexible cable anchoring section at the edge of the silicon island.

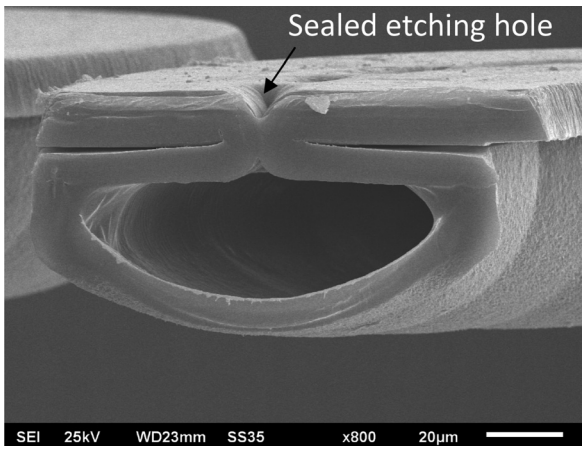

FIG. 6. Cross sectional SEM image of the flexible cable.

that the margin between the oxide layer and edge of silicon island ensures that there is no rigid layer at the edge of the silicon island. It can be observed that the micro-cushion/channel structure underneath the metal trace extends into the silicon island, helping to minimize the stress experienced by the metal trace at the rigid silicon edge. To avoid short circuit to the silicon, the channel needs to be further extended under the silicon oxide layer a certain distance.

Figure 6 shows the cross sectional image of the flexible cable. Note that the peeling off between the flat parylene layer and parylene channel is caused by the mechanical force occurred during sample preparation (cutting). The metal trace cannot be viewed clearly in this image. However, based on the fabrication process, it is right between the flat parylene layer and the parylene channel. The cross section of a sealed etching hole can also be observed in Fig. 6.

Finite element simulations were conducted to show that the new design with the microcushion structure has much lower stress compared with the original flat cable design during processing. When temperature varies during microfabrication processing, since different components (e.g., Si, SiO_2, Al, and Parlyene-C) have different thermal expansion coefficients, thermal stress is generated. We modeled this thermal stress problem by applying a temperature load of $-50\,^{\circ}\mathrm{C}$ uniformly throughout the model that consists of Si, SiO_2, Al, and Parlyene-C. The material properties are $E_{\mathrm{Si}} = 112\,\mathrm{GPa}$, $\nu_{\mathrm{Si}} = 0.28$, $\alpha_{\mathrm{Si}} = 2.6 \times 10^{-6}\ \mathrm{K}^{-1}$, $E_{\mathrm{SiO2}} = 75\,\mathrm{GPa}$, $\nu_{\mathrm{SiO2}} = 0.17$, $\alpha_{\mathrm{SiO2}} = 0.5 \times 10^{-6}\ \mathrm{K}^{-1}$, $E_{\mathrm{Al}} = 70\,\mathrm{GPa}$, $\nu_{\mathrm{Al}} = 0.35$, $\alpha_{\mathrm{Al}} = 23 \times 10^{-6}\ \mathrm{K}^{-1}$, $E_{Parlyene-C} = 3.2\,\mathrm{GPa}$, $\nu_{Parlyene-C} = 0.4$, $\alpha_{Parlyene-C} = 35 \times 10^{-6}\ \mathrm{K}^{-1}$, where E is the elastic modulus, ν is the Poisson's ratio, α is the coefficient of thermal expansion, and the subscripts denote different materials. Symmetric boundary conditions were applied. The finite element package ABAQUS was utilized in the simulation. For the traditional flat cable design, 13 306 two-dimensional plane stress elements (CPS4R) were used. For the new design, 20 464 CPS4R elements were used. Tie constraints were used to link all components. Figure 7 shows the contour of the von Mises stress close to the jointing points between Si island and the Parlyene cable for both designs. It is clear that for the traditional design, the maximum stress occurs at the Al layer and there are a few orders of magnitude difference on von Mises stress. For the design of the cushioned cable, the stress field is fairly uniform and the maximum stress (about 7.2 MPa) is about 2 orders of magnitude lower than the traditional design (about 170 MPa). The simulations show that the flexible cable design can significantly reduce the stress during processing.

Data on the functionality of the device were quantified by measuring the resistance of the metal trace dynamically as the axial length of the device was varied. The length variation was controlled using a home-built motorized stage (inset of Fig. 8). The length of the device was changed in $\sim 22.25\,\mu\mathrm{m}$ increments, and the electrical resistance between two connected contact pads was measured continuously by a digital millimeter (Agilent 34401A) with a sampling rate of 200 ms. The data was transferred to a computer via a GPIB card (NI GPIB-USB-HS). At least 50 data points were averaged together after the reading appeared to reach a plateau to form each data point on a generated resistance vs. strain plot shown in Figure 8. It can be observed that the resistance remained almost constant when the strain is $< \pm 10\%$. In many cases, test devices were driven until their electrical contacts failed, i.e., resistance readings indicated an open circuit. We took these as the failure points. When operated in stretching only increments, we achieved a maximum strain of 45%. Compression only operation suggested that the maximum compressive strain could be very high, and is at least higher than 50%. It is worth noting that in this proof-of-concept work, the shape of the serpentine cable is not optimized. The maximum strain may be significantly increased by optimizing the design.

The enhanced stretchability of the new flexible cable design was verified by finite element simulations using ABAQUS. Identical strains were applied to both traditional flat cable design and the new cushioned design in the longitudinal direction. The simulation results illustrate that the maximum stress occurs at the boundary of the silicon island for both cases. The stress is non-uniform and there are a few orders of magnitude difference on von Mises stress for the traditional design. Comparatively, the stress field is fairly

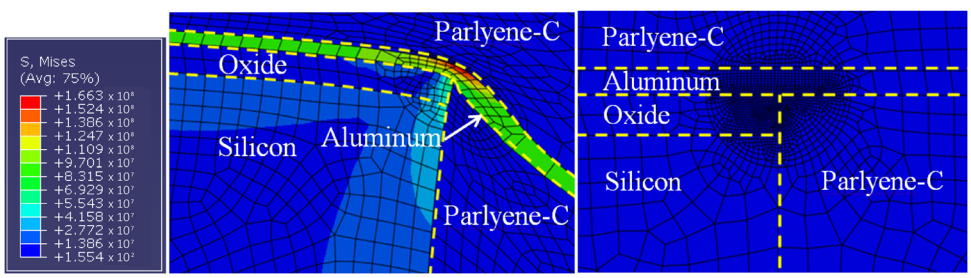

FIG. 7. Contour of von Mises stress upon a temperature load for (a) the traditional design and (b) the new cushioned design.

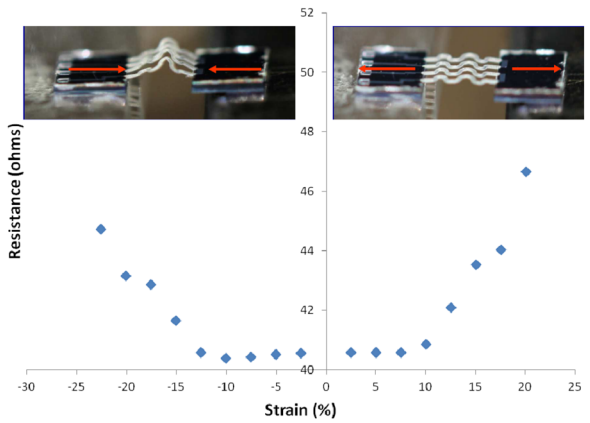

FIG. 8. Resistance of a strain gauge as a function of strain. Negative strain means compression and positive strain means stretching, as illustrated in the insets.

uniform for the cushioned design and the maximum stress is about one order of magnitude smaller than that of the traditional design. The simulations, again, show that the new design can significantly increase the stretchability.

A robust micro cable structure for silicon island based flexible skins has been demonstrated. With this structure, the metal traces are buffered with cushions at the edge of the silicon island, significantly reducing the stress concentration. In addition, this structure has a number of other advantages. First, the incorporation of this cushion structure is compatible with the micro-channel fabrication. Therefore, micro-channels can be simultaneously integrated into the flexible skins. Second, after forming this cushion/channel structure, the metal traces are completely encapsulated by parylene, avoiding coating of another layer of polymer after backside deep reactive ion etching. Third, this structure makes the flexible cables mechanically much stronger than flat cables. In conclusion, this structure can significantly increase the reliability of the silicon island based flexible devices from multiple aspects, and simultaneously incorporate more functionalities into the flexible device (e.g., micro-channels). Consequently, we believe that the silicon island based flexible skin technology could have additional significant impacts on a broader range of applications.

This material is based upon work partially supported by the National Science Foundation under Grant Nos. 0747620 and 1028564. Any opinions, findings, and conclusions or recommendations expressed in this material are those of the author(s) and do not necessarily reflect the views of the National Science Foundation. The microfabrication was carried out in the nFAB cleanroom at Wayne State University and LNF at University of Michigan, Ann Arbor.

[1]F. Fortunato, I. Ferreira, F. Giuliani, and R. Martins, Sens. Actuators, A **86**(3), 182 (2000).
[2]T. Stieglitz, H. Beutel, and J. U. Meyer, Sens. Actuators A **60**(1–3), 240 (1997).
[3]M. Boucinha, P. Brogueira, V. Chu, and J. P. Conde, Appl. Phys. Lett. **77**(6), 907 (2000).
[4]S. H. Ko, H. Pan, C. P. Grigoropoulos, C. K. Luscombe, J. M. J. Frechet, and D. Poulikakos, Nanotechnology **18**(34), 345202 (2007).
[5]H. Minemawari, T. Yamada, H. Matsui, J. Tsutsumi, S. Haas, R. Chiba, R. Kumai, and T. Hasegawa, Nature **475**(7356), 364 (2011).
[6]T. Sekitani, Y. Noguchi, U. Zschieschang, H. Klauk, and T. Someya, Proc. Natl. Acad. Sci. U.S.A. **105**(13), 4976 (2008).
[7]T. H. J. van Osch, J. Perelaer, A. W. M. de Laat, and U. S. Schubert, Adv. Mater. **20**(2), 343 (2008).
[8]B. Y. Ahn, E. B. Duoss, M. J. Motala, X. Guo, S.-I. Park, Y. Xiong, J. Yoon, R. G. Nuzzo, J. A. Rogers, and J. A. Lewis, Science **323**(5921), 1590 (2009).
[9]K. J. Lee, J. Lee, H. D. Hwang, Z. J. Reitmeier, R. F. Davis, J. A. Rogers, and R. G. Nuzzo, Small **1**(12), 1164 (2005).
[10]E. Menard, K. J. Lee, D. Y. Khang, R. G. Nuzzo, and J. A. Rogers, Appl. Phys. Lett. **84**(26), 5398 (2004).
[11]H. C. Yuan, Z. Q. Ma, M. M. Roberts, D. E. Savage, and M. G. Lagally, J. Appl. Phys. **100**(1), 013708 (2006).
[12]K. J. Lee, M. J. Motala, M. A. Meitl, W. R. Childs, E. Menard, A. K. Shim, J. A. Rogers, and R. G. Nuzzo, Adv. Mater. **17**(19), 2332 (2005).
[13]D. H. Kim, N. S. Lu, R. Ma, Y. S. Kim, R. H. Kim, S. D. Wang, J. Wu, S. M. Won, H. Tao, A. Islam, K. J. Yu, T. I. Kim, R. Chowdhury, M. Ying, L. Z. Xu, M. Li, H. J. Chung, H. Keum, M. McCormick, P. Liu, Y. W. Zhang, F. G. Omenetto, Y. G. Huang, T. Coleman, and J. A. Rogers, Science **333**(6044), 838 (2011).
[14]J. Viventi, D.-H. Kim, J. D. Moss, Y.-S. Kim, J. A. Blanco, N. Annetta, A. Hicks, J. Xiao, Y. Huang, D. J. Callans, J. A. Rogers, and B. Litt, Sci. Transl. Med. **2**(24), 24ra22 (2010).
[15]D. H. Kim, N. S. Lu, R. Ghaffari, Y. S. Kim, S. P. Lee, L. Z. Xu, J. A. Wu, R. H. Kim, J. Z. Song, Z. J. Liu, J. Viventi, B. de Graff, B. Elolampi, M. Mansour, M. J. Slepian, S. Hwang, J. D. Moss, S. M. Won, Y. G. Huang, B. Litt, and J. A. Rogers, Nat. Mater. **10**(4), 316 (2011).
[16]Y. Xu, F. Jiang, S. Newbern, A. Huang, C. M. Ho, and Y. C. Tai, Sens. Actuators, A **105**(3), 321 (2003).
[17]Y. Xu, Y. C. Tai, A. Huang, and C. M. Ho, J. Microelectromech. Syst. **12**(5), 740 (2003).
[18]R. B. Katragadda and Y. Xu, Sens. Actuators, A **143**(1), 169 (2008).
[19]J. John, Y. F. Li, J. S. Zhang, J. A. Loeb, and Y. Xu, J. Micromech. Microeng. **21**(10), 105011 (2011).
[20]Y. Li, H. Tu, R. Iezzi, P. Finlayson, and Y. Xu, J. Micromech. Microeng. **21**(11), 115005 (2011).
[21]K. Zheng, W. Khalid, Z. Wang, Y. Li, R. B. Katragadda, Y. Zhao, Q. Lin, and Y. Xu, Open Opt. J. **2**(8), 86 (2008).
[22]R. Katragadda, Z. Wang, W. Khalid, Y. Li, and Y. Xu, Appl. Phys. Lett. **91**(8), 083505 (2007).
[23]Y. Li, Q. Zheng, Z. Wang, R. Katragadda, W. Khalid, R. P. Panguluri, B. Nadgorny, P. M. Hoffmann, and Y. Xu, Sens. Lett. **6**(2), 299 (2008).